



## SHEAR LOCALIZATION IN HIGH-STRAIN-RATE DEFORMATION OF GRANULAR ALUMINA

V. F. NESTERENKO†, M. A. MEYERS and H. C. CHEN

Department of Applied Mechanics and Engineering Sciences, University of California, San Diego, La Jolla, CA 92093, U.S.A.

(Received 27 June 1995)

**Abstract**—Dynamic deformation of densified granular alumina of two different particle sizes was investigated by the radial symmetric collapse of a thick-walled cylinder. The densified granular alumina was used to model the flow in ballistic impact and penetration of fragmented ceramic armor. Shear localization was a well developed deformation mode at an overall radial strain of  $\sim 0.2$ – $0.4$  and strain rate of  $10^4$  s $^{-1}$ . The following qualitative features of shear bands were established:

- Shear bands have clear boundaries and their thickness does not depend on the initial particle size and has a typical value  $\sim 10$   $\mu$ m.
- The structure of the shear bands was dependent on initial particle size, suggesting differences in the mechanisms of flow. For the  $\sim 4$   $\mu$ m alumina, comminution (break-up) and softening of particles were observed. For the  $\sim 0.4$   $\mu$ m particles, a peculiar structure consisting of a central crack with two lateral cracks was formed.
- Distributions of shear bands and displacement magnitudes were dependent on initial particle size.

The observed differences in powder behavior are associated with different mechanisms of powder repacking. For large particles ( $\sim 4$   $\mu$ m), additional hardening resulting from microfracture and subsequent repacking of different size particles in the powder takes place. The small-sized ( $\sim 0.4$   $\mu$ m) ceramic does not go through the particle fracturing stage and the hardening is due to “classical” repacking.

### 1. INTRODUCTION

Ballistic impact of ceramic armor generates a range of phenomena that are still poorly understood. Shockey *et al.* [1] performed recovery experiments, which clearly show the different regimes of damage observed. Viechnicki [2] divided the levels of damage into three classes: a comminuted zone produced by shock waves; radial cracks produced by the expanding stress wave; and cracks generated by the reflection of the compressive pulses at the back surface of the armor plate. In the comminuted zone, the high-amplitude shock waves create stresses that exceed the strength of the ceramic. It is, as a result, finely divided into fragments. This comminuted (or finely fragmented) region is extremely important in the overall penetration mechanism, since it has to be ejected from the target in order for penetration to proceed. Mescall [3] postulated the existence of this region, based on hydrocode computations; experimental studies have confirmed its existence. Meyers [4] reviewed these mechanisms. The ejection of the comminuted, or “Mescall”

zone, from the target requires large deformations of the granular material. The objective of this paper is to report results of experiments especially designed to subject dense and fragmented ceramics to large “plastic” deformation at high strain rates, representing in a realistic manner the behavior of the ceramic adjacent to a penetrator. The fragmented ceramic was modeled by precompact alumina powder.

Shear localization is an important deformation mode in the quasi-static mechanical response of granular materials; it has been widely investigated both from an analytical and experimental point-of-view [5–16]. Rudnicki and Rice [5] developed a general formulation for shear localization in pressure-sensitive dilatant materials, of which granular materials are a special case. There are no reports, to the authors’ knowledge, on shear localization under high-strain-rate loading of granular materials.

### 2. EXPERIMENTAL PROCEDURE

Alumina powders with two particle sizes were used in this investigation. These Al $_2$ O $_3$  powders had a purity level of 99.97% and contained trace amounts of Na, Si, Ca, Ga, Fe, Mg, Ti and Zn. The powders

†On leave from Lavrentyev Institute of Hydrodynamics, Russian Academy of Sciences, Novosibirsk, 630090, Russia.

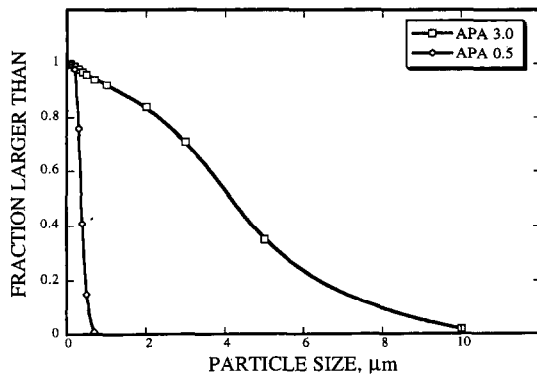


Fig. 1. Cumulative particle size distribution for CERALOX alumina.

were donated by CERALOX and have two designations:

- (a) APA 3.0—median particle size:  $4.17 \mu\text{m}$ ;  
surface area:  $1.5 \text{ m}^2/\text{g}$ ;
- (b) APA 0.5—median particle size:  $0.37 \mu\text{m}$ ;  
surface area:  $8.9 \text{ m}^2/\text{g}$ .

The particle size distributions are given in Fig. 1. The two materials will be denoted “small” (or  $\sim 0.4 \mu\text{m}$ ) and “large” (or  $\sim 4 \mu\text{m}$ ) in the subsequent discussion.

The densification and deformation of the aluminas were carried out using the axial collapse of a thick-walled-cylinder within which the powder was placed. This thick-walled-cylinder method had been successfully used previously for research on solid [17] and porous materials [18, 19]. The experimental configuration [18, 19] used to generate controlled and prescribed shear localization in porous samples is shown in Fig. 2. The process has two stages: (a) densification of the powder [Fig. 2(a)]; (b) deformation of the densified powder [Fig. 2(b)]. The alumina powder

with a density of  $1.5 \text{ g/cm}^3$  ( $\sim 38\%$  of the theoretical value) was initially placed in a tubular cavity between a central copper rod (diameter 16 mm) and an outer copper tube (inner diameter 20 mm and outer diameter 31 mm). An explosive [explosive 1, mixture of ammonite and sand in 3:1 volume ratio, Fig. 2(a)] with a low detonation velocity ( $3.2 \text{ km/s}$ ) was used to densify this mixture to a density of  $3.35 \text{ g/cm}^3$  ( $\sim 84\%$  of the theoretical value of  $3.98 \text{ g/cm}^3$ ). Detonation was initiated at the top of the charge and propagated along the cylinder axis. Only small initiation sites of shear localization (Fig. 3) were observed after this stage because the overall plastic deformation is sufficiently small (final diameter of inner surface of driving copper cylinder,  $r_{10}$ , is equal to 17.9 mm). This stage produced mainly densification of the powder. The small step (marked by an arrow) seen in the shear copper container is indicative of the initiation of shear localization.

A cylindrical hole with 11 mm diameter was drilled along the longitudinal axis of the copper rod and this composite cylinder was collapsed by the detonation of a second cylindrical explosive charge [explosive 2 (ammonite), Fig. 2(b)] with a detonation velocity of  $4.2\text{--}4.4 \text{ km/s}$ , an initial density of  $1 \text{ g/cm}^3$ , and an outer diameter of 60 mm. This second explosive event produced significant plastic deformation in the densified porous layer which was highly localized in shear bands and not homogeneously distributed [Fig. 2(c)]. It is worthwhile mentioning that shear localization during explosive compaction of ceramic powders in the cylinder geometry was observed by Prummer [20].

### 3. RESULTS AND DISCUSSION

The general view of the collapsed ceramic cylinders is shown in Fig. 4. Profuse shear localization can be

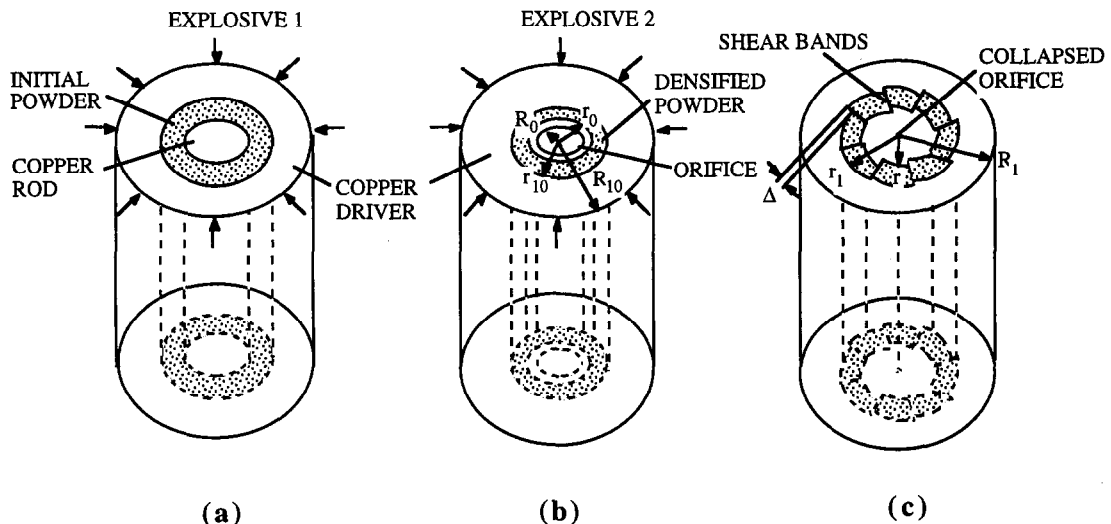


Fig. 2. Experimental set-up for densification and plastic deformation of ceramic: (a) configuration for densification; (b) configuration for deformation of densified alumina (notice axial orifice that enables large plastic strains in copper containers); (c) final configuration with schematic representation of shear localization.



Fig. 3. Nucleation of shear in “large” grain powder on the densification stage, marked by the appearance of a kink on the outer surface of the ceramic layer (after compression by explosive 1).

seen for both particle sizes. The spacing between the shear localization regions, that make an angle of  $45^\circ$  with the radial direction, is fairly regular, and both clockwise and counterclockwise directions are observed. The average values of internal radii  $r$  were equal to 5.9 mm after collapse for both powders. The external radii  $r_1$  of the porous layer after collapse were equal to 7.3 and 7.4 mm for large and small particles, respectively. The initial values are 8 mm ( $r_0$ ) and 9 mm ( $r_{10}$ ) for both powders. From these data it is possible to conclude that the deformation undergone by the powders with different initial particle sizes is nearly identical.

The quantitative determination of the overall material strain can be obtained from the strains in the incompressible copper shell driving the collapse process. The radial and tangential engineering strains ( $e_{rr}$  and  $e_{\varphi\varphi}$ ) for an incompressible material, before the onset of localization, can be estimated knowing the initial and final radii,  $\rho_0$  and  $\rho$ , at a general point:

$$e_{rr} = \frac{\rho_0}{\rho} - 1, \quad e_{\varphi\varphi} = \frac{\rho}{\rho_0} - 1. \quad (1)$$

The strains in the surfaces of copper cylinders restricting the porous tubular layer can be found from equation (1). The final radii  $\rho$  and  $R$  (or  $R_1$ ) and initial radius  $R_0$  (or  $R_{10}$ ) [Fig. 2(b)] are experimentally measured and the value of  $\rho_0$ , which corresponds to a preselected value of  $\rho$ , can be calculated using equation (2) (conservation of mass):

$$\rho_0^2 = \rho^2 + R_0^2 - R^2 = \rho^2 + R_{10}^2 - R_1^2 \quad (2)$$

where  $R$  and  $R_1$  are final radii of the inner hole and outer cylinder surface.

The overall strain in copper at the boundary with the porous layer outside the shear localization region can be estimated using equation (1). After the first explosive event one obtains: at  $\rho = r_{10}$ ,  $e_{rr} \cong 0.12$  and  $e_{\varphi\varphi} = -0.11$ . After the second explosive event at  $\rho = r_1$ ,  $e_{rr} \cong 0.23$ ,  $e_{\varphi\varphi} \cong -0.18$ ; at  $\rho = r$ ,  $e_{rr} \cong 0.37$  and  $e_{\varphi\varphi} \cong -0.27$ . The dependence of effective strain rate on time is presented in Fig. 5 for the outer and inner layers of alumina. The difference in strain rates for these two points is not significant and the average strain rate can be considered to be  $2.5 \times 10^4 \text{ s}^{-1}$ . Note that the deformation in copper [17] under these conditions is homogeneous and that is why the beginning of shear localization is determined completely by the ceramic layer. The strain rates were obtained from calculations based on velocity records of the inner wall velocity [17–19].

The distribution of the clockwise and counterclockwise displacements in the shear bands is depicted in Fig. 6. They apply to the same interval in spite of being plotted sequentially in the corresponding intervals of  $50 \mu\text{m}$  marked in abscissa; for the  $0\text{--}50 \mu\text{m}$  interval the occurrence of displacements below  $25 \mu\text{m}$  is negligible. Both distributions are close for small displacements ( $< 50 \mu\text{m}$ ), but are drastically different for larger displacements. The  $0.4 \mu\text{m}$  alumina has a “tail” in the region of large displacements, which is absent for the  $4 \mu\text{m}$  alumina. Figures 4 and 6 enable the conclusion to be made that, despite

the same experimental configuration for both materials, the shear-band patterning is qualitatively different. The material with "small" particles is more unstable to shear localization whereas the material with "large" particle sizes deforms uniformly with shear bands arising only at a later stage of collapse. As a consequence of a more severe loss of strength (softening) for the  $0.4\ \mu\text{m}$  alumina, large displacements ( $\Delta$ ) tend to be produced.

The partition of the strains due to the shear bands ( $e_s$ ) and homogeneous deformation ( $e_h$ ) was computed for the two aluminas according to the expression:

$$e_t = e_h + e_s, \quad (3)$$

$e_t$  is the total tangential strain imparted by the geometry. Taking an average value between the internal and external radius, one obtains:

$$e_t = -0.22.$$

The strain due to localization is obtained by taking the tangential component of the summation of displacements,  $\Delta$ , [see Fig. 2(c)],

$$e_s = -\frac{\sqrt{2}\Sigma\Delta}{2\pi(r_{10} + r_0)}. \quad (4)$$

This enables the calculation of the homogeneous strain,  $e_h$ :

$$e_h = e_t + \frac{\sqrt{2}\Sigma\Delta}{2\pi(r_{10} + r_0)}. \quad (5)$$

The strains due to shear,  $e_s$ , are  $-0.08$  and  $-0.04$  for the small and large particle-sized materials, respectively. Thus, the homogeneous strains,  $e_h$ , are equal to  $-0.14$  and  $-0.18$  for the small and large particle-sized materials, respectively. One may conclude that localization occurs earlier for the "small" particle-sized alumina. This will be discussed later. It is also possible to estimate the average distance between shear bands at the onset of localization. This

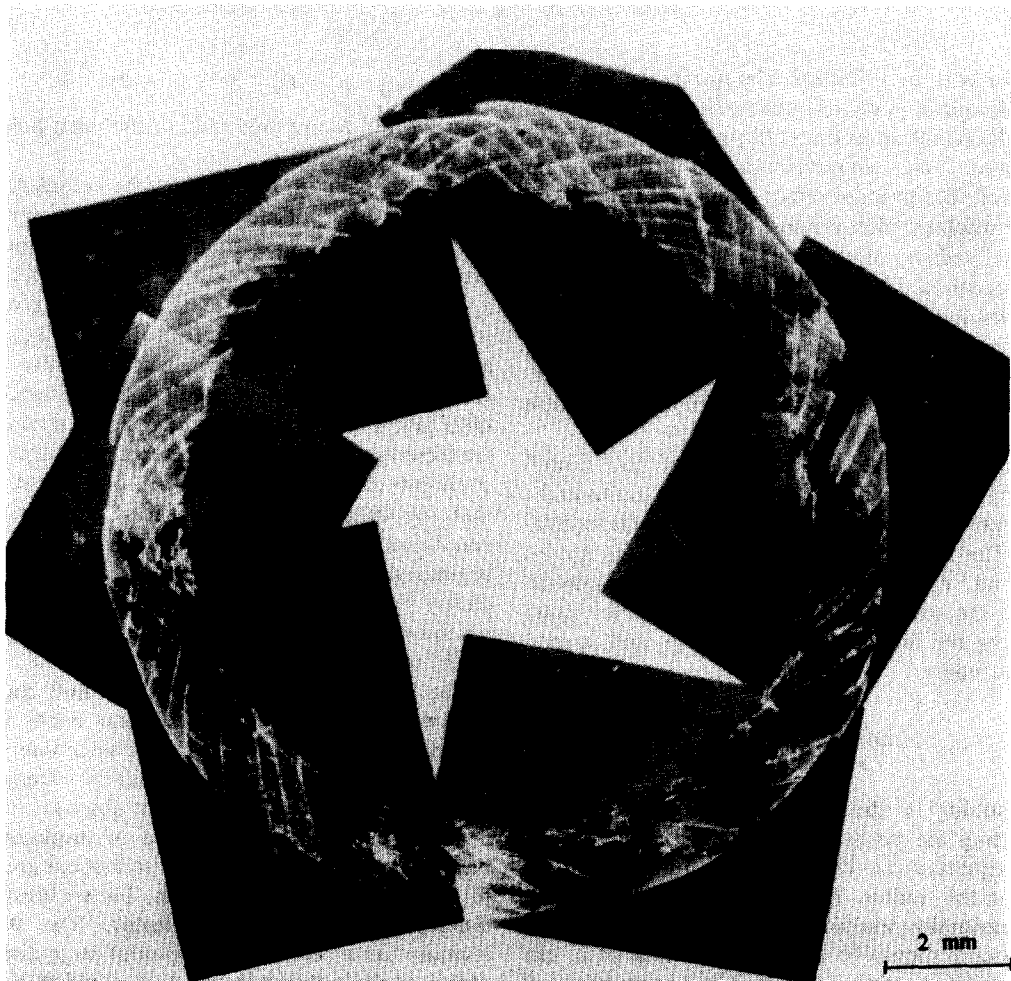


Fig. 4(a).—See caption opposite.

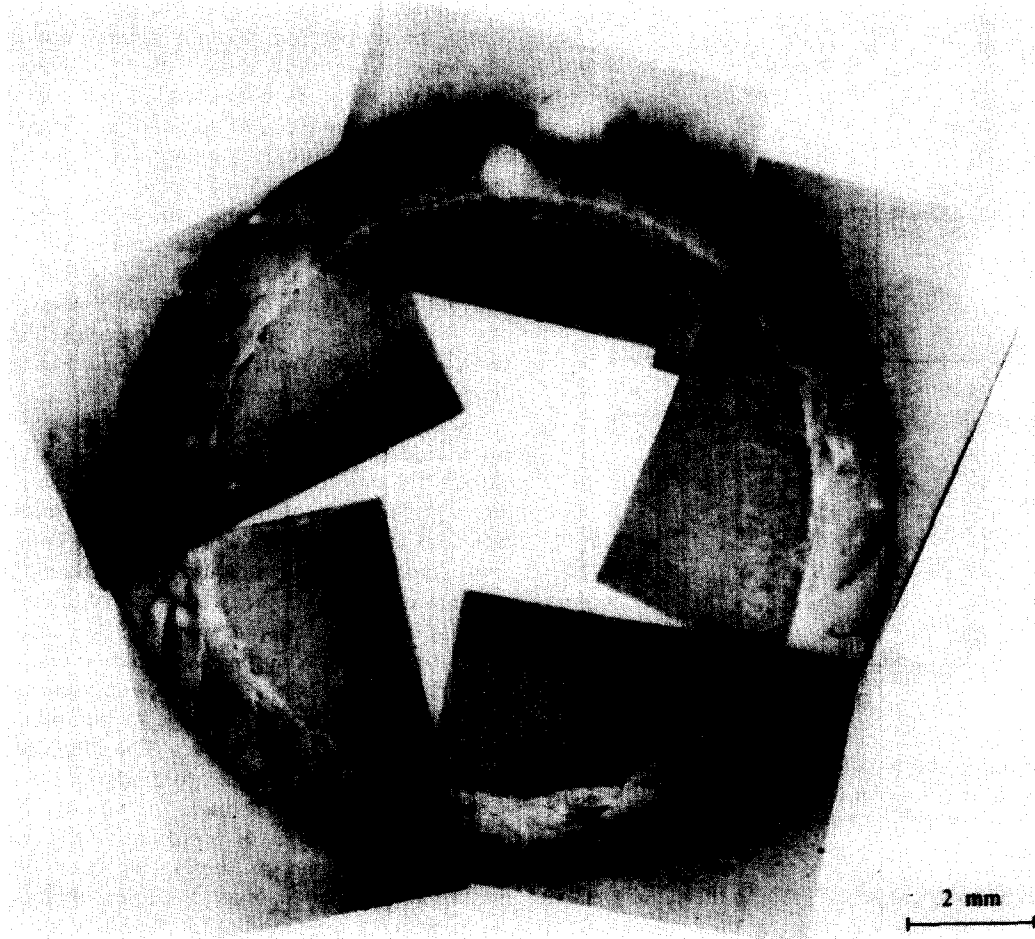


Fig. 4. Overall view of the ceramic layer after collapse process: (a) particle size  $\sim 0.4 \mu\text{m}$ ; (b) particle size  $\sim 4 \mu\text{m}$ .

is obtained by estimating the radius  $r_i$  at the onset of localization (from the initial value of  $r_{10}$  and value of  $e_h$  and by dividing the number of bands,  $N$ , by the inner circumference ( $2\pi r_i$ ):  $L = 2\pi r_i / \sqrt{2N}$ . Note the introduction of the correction for the orientation of the bands. This assumes that all bands are generated simultaneously. The values of  $r_i$  are 6.9 and 6.6 mm

for the 0.4 and  $4 \mu\text{m}$  particles, respectively. The corresponding spacings  $L$ , are 0.49 and 0.61 mm. The minimum spacing between shear bands has been treated by Grady and Kipp [21] and Ockendon and Wright [22]; similar analyses could be extended to granular materials, where the principle softening modes are not thermal. It is interesting that, despite essential differences between granular alumina and monolithic titanium and stainless steel, the spacings are of the same order of magnitude [23]. At present, there is no satisfactory theoretical treatment.

The shear band structures are presented in Figs 7 and 8 for small ( $0.4 \mu\text{m}$ ) particles. The evolution of the shear band structure with displacement for "small" particles is shown in Fig. 7. It is interesting that shear-band thickness ( $\sim 10\text{--}20 \mu\text{m}$  or  $20\text{--}40$  maximum particle sizes) does not depend on the displacement [Figs 7(a)–(c)]. As the displacement increases, cracking becomes more prominent; a central crack is seen in the shear band with largest displacement, which starts at the intermediate stage [Fig. 7(b)]. Particle agglomeration is evident inside

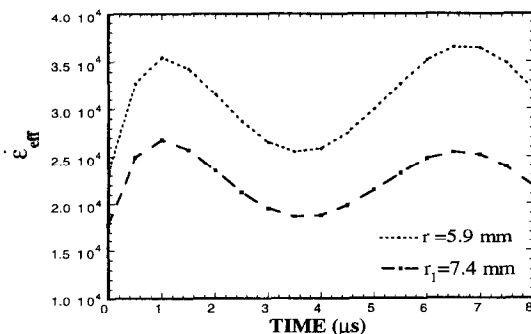


Fig. 5. Effective strain rate for inside and outside boundary layers of collapsing ceramic layer.

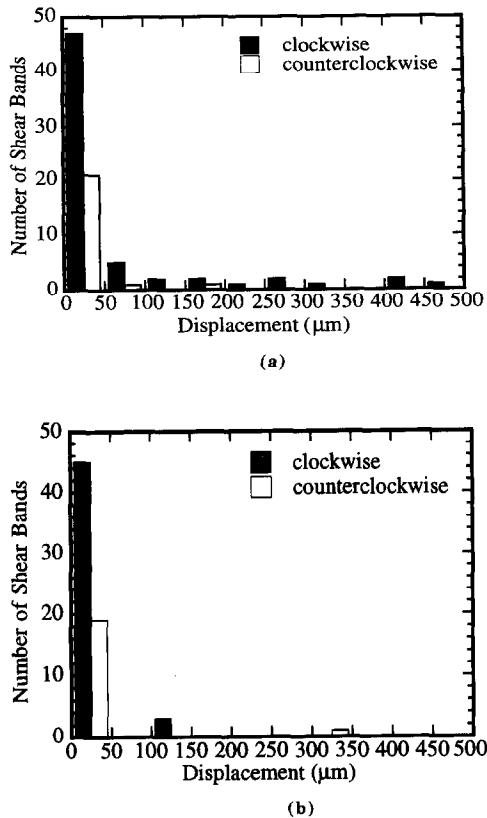


Fig. 6. Distribution of shear bands (clockwise and counterclockwise) as a function of displacement  $\Delta$  on the outer surface of collapsed ceramic layer: (a)  $0.4 \mu\text{m}$ ; (b)  $4 \mu\text{m}$ .

the shear band [Figs 7(a)–(c)]. At the same time, as evident from Figs 8(a) and (b), the average size of particles between the central crack and outside boundary of shear band is close to the initial value. One can conclude that, as the displacement in shear band proceeds, a process of agglomeration of the ceramic occurs, providing new structural elements with typical sizes of the order of the shear-band thickness.

The structure of the shear band for the large ( $4 \mu\text{m}$ ) particles is shown in Fig. 9. The shear-band thickness [Figs 9(a)–(c)] is of the same order of magnitude ( $11 \mu\text{m}$  or approximately three average particle sizes) as the thickness for small particles [Figs 7(a)–(c)]. This result clearly demonstrates that the particle size cannot be considered as a scaling parameter for shear-band width in precompacted granular alumina, under high-strain-rate deformation. This behavior is in contrast with shear-band thickness in tapped granular material, without preliminary densification [6, 12, 24]. Vardoulakis [6] reported experimental measurements of shear-band thickness between 10 and 15 times the mean particle diameter. The superimposed hydrostatic component of stress is relatively high in the thick-walled-cylinder geometry. To a first approximation, it can be taken as 2 GPa. This hydrostatic stress influences the deformation processes by in-

creasing the frictional effects and the resultant thermal excursion.

Although the thicknesses are similar, the structure of the band and the fracture pattern are quite different. Figure 9(a) shows the band for the  $4 \mu\text{m}$  material; it is composed of material that is clearly comminuted. The particle size is considerably reduced. Figure 9(b) shows the band for a higher displacement ( $\Delta = 50 \mu\text{m}$ ). The particles show rounded edges and these features are suggestive of high temperatures and plastic flow within the particles. At even higher displacements [Fig. 9(c);  $\Delta = 330 \mu\text{m}$ ] cracking appears as a prominent feature. Regions adjacent to the cracks exhibit particle fracturing, which is evident in Fig. 9(d); arrows indicate fractured particles.

The difference in shear-band structure between the two aluminas can be rationalized by the absence of particle fracture for the  $0.4 \mu\text{m}$  alumina. This is a direct consequence of fracture mechanics since the flaw sizes are limited by the particle sizes. To a first approximation, the stress required to fracture  $0.4 \mu\text{m}$  particles is three times the stress required to fracture  $4 \mu\text{m}$  particles [ $\sigma = K_{IC}(\pi a)^{-1/2}$ ]. This fracturing of the  $4 \mu\text{m}$  particles during deformation leads to an improved repacking, which is a mechanism of deformation. Therefore, the stage of homogeneous macrodeformation is extended. The hypothetical stress–strain response of the two aluminas is shown in Fig. 10. The main features of the two curves are shown. The onset of softening (which many investigations equate to shear-band initiation) is marked as  $\gamma_c$ ; it corresponds to  $e_h$  in equation (5). It is interesting to observe that the strains at the onset of localization are close to the ones observed by Desrues *et al.* [11]: they observed, for granular material, in an axisymmetric compression test, that the onset of localization occurred at  $e \cong -0.15$ . In Fig. 10, the more pronounced hardening of the  $4 \mu\text{m}$  particles is attributed to fracturing, repacking and filling the interparticle spaces with the comminuted material. The greater incidence of shear bands with larger displacement,  $\Delta$ , for the  $0.4 \mu\text{m}$  alumina is also rationalized in Fig. 10. The softening within the  $0.4 \mu\text{m}$  shear bands is more drastic and is associated with the formation of a crack structure, whereas the  $4 \mu\text{m}$  alumina undergoes a more gradual softening.

It should be mentioned that Rudnicki and Rice [5] showed that, under conditions of plane strain for “non-associated” plasticity, the localization process can occur even if the material strain hardens. This has been experimentally observed for sand by Desrues *et al.* [11]. The distribution of shear-band displacements ( $\Delta$ ) for the small-particle material agrees qualitatively with predictions based on computer calculations by Poliakov and Herrman [25]. They demonstrated that shear displacements follow a power law; this is a manifestation of self-organized criticality.

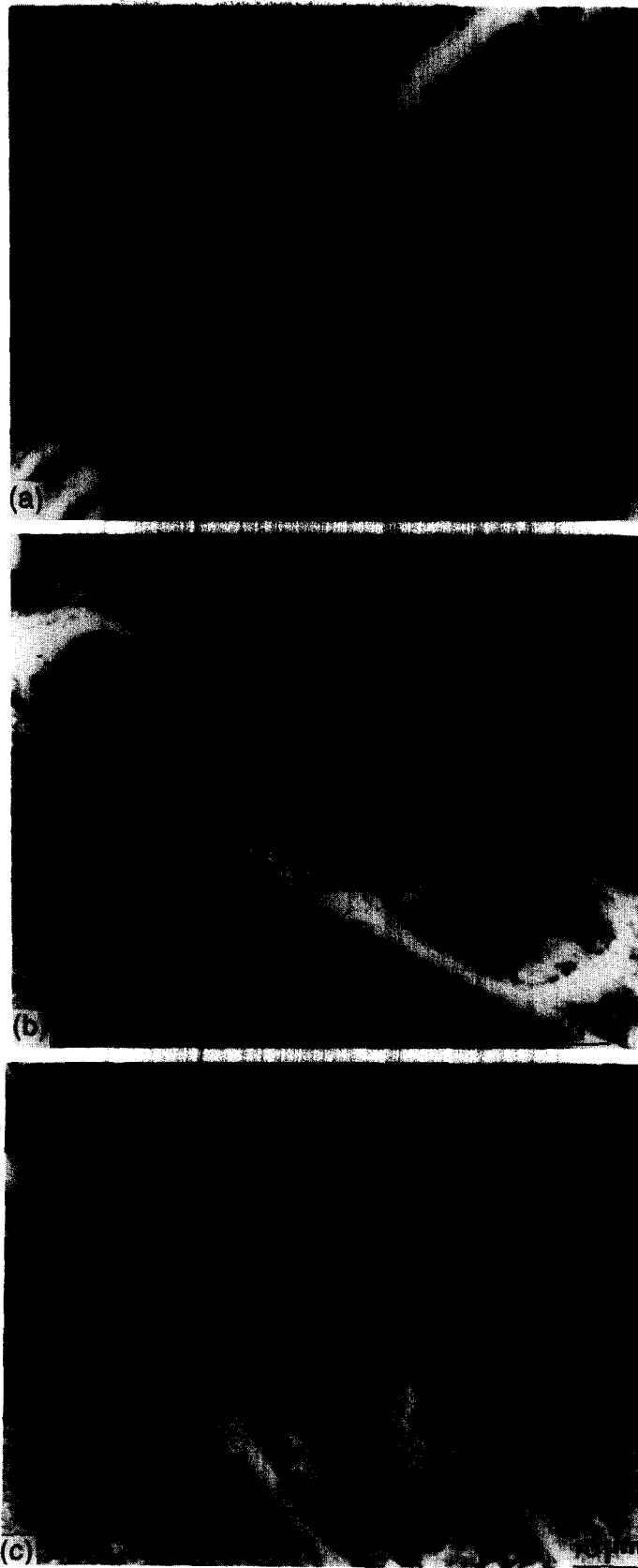


Fig. 7. Dependence of the shear band structure on displacement ( $\Delta$ ) in small ( $0.4 \mu\text{m}$ ) particle powder:  
(a)  $\Delta = 10 \mu\text{m}$ ; (b)  $\Delta = 120 \mu\text{m}$ ; (c)  $\Delta = 570 \mu\text{m}$ .

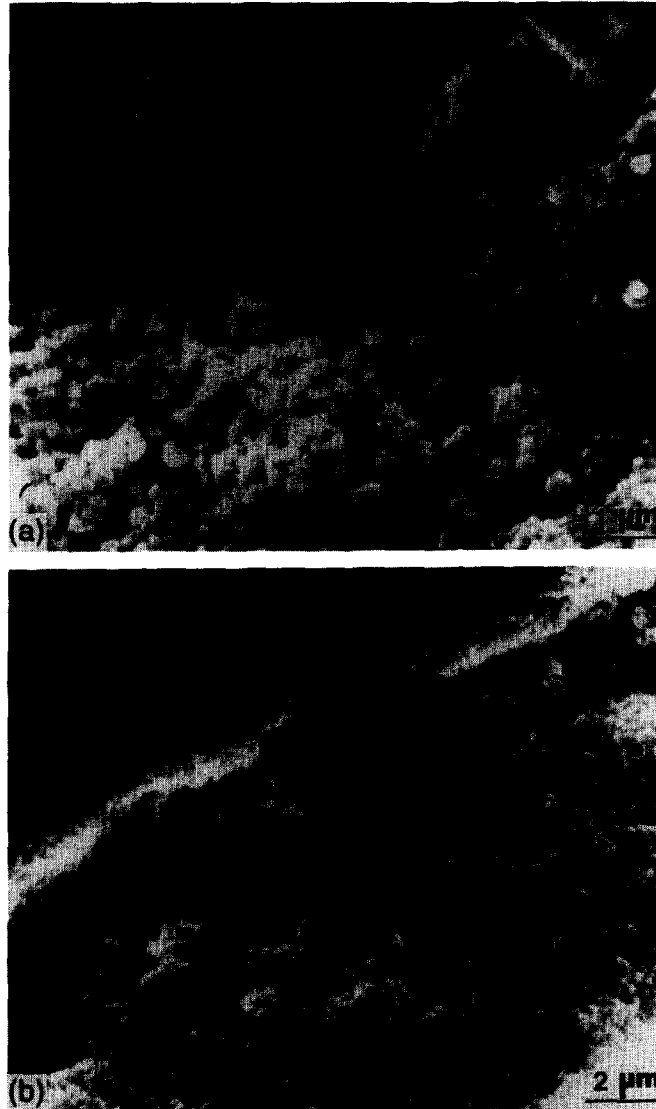


Fig. 8. Structure inside different regions of the shear band in small ( $0.4 \mu\text{m}$ ) particle powder, corresponding to Fig. 7(c) ( $\Delta = 570 \mu\text{m}$ ): (a) material adjacent to the central crack (in left top corner); (b) material adjacent to the shear boundary.



Fig. 9. Dependence of the shear band structure on displacement ( $\Delta$ ) in large ( $4 \mu\text{m}$ ) particle powder: (a)  $\Delta = 30 \mu\text{m}$ ; (b)  $\Delta = 50 \mu\text{m}$ ; (c)  $\Delta = 330 \mu\text{m}$ ; (d) cracks in particles adjacent to the shear boundary ( $\Delta = 330 \mu\text{m}$ ).

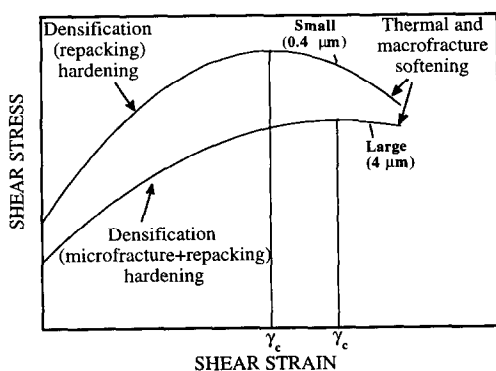


Fig. 10. Hypothetical stress-strain curves for shear deformation of densified granular materials with two particle sizes.

The relative effects of thermal softening, macrocrack propagation and dilatation within the localization regions are not well understood at present. However, the results reported herein are novel and demonstrate the need for further study of damage evolution inside shear bands.

#### 4. CONCLUSIONS

- (1) Shear localization is an important mechanism in high-strain-rate-deformation of densified porous alumina.
- (2) The evolution of shear bands is dependent on particle size. The  $4\ \mu\text{m}$  material exhibits a large number of bands with similar ( $< 50\ \mu\text{m}$ ) displacements, whereas the shear bands within the  $0.4\ \mu\text{m}$  material have a wide distribution of displacements ( $50\text{--}500\ \mu\text{m}$ ). These differences are due to different softening mechanisms within the bands.
- (3) The structure within the shear band is highly dependent on particle size. For the  $0.4\ \mu\text{m}$  alumina, a network of cracks along the direction and perpendicular to the shear bands is formed. For the  $4\ \mu\text{m}$  alumina, the principal feature is the presence of comminuted material within the band.
- (4) The shear-band thickness is not significantly affected by particle size or displacement and is approximately  $10\text{--}20\ \mu\text{m}$ . This is in contrast with granular materials with tapped density, which exhibit shear-band thicknesses which are a multiple ( $10\text{--}20$ ) of the particle size.

*Acknowledgements*—This research is supported by the U.S. Army Research Office, Contract DAAH 04-94-G-0314 and by the U.S. Office of Naval Research, Contract N00014-94-1-1040. The authors wish to acknowledge the valuable help in conducting experiments by Dr M. P. Bondar and Ya. L. Lukyanov (Lavrentyev Institute of Hydrodynamics, Novosibirsk, Russia), as well as Prof. R. J. Clifton (Brown University) for discussions. The generosity of

CERALOX in donating the powders for this research is gratefully appreciated.

#### REFERENCES

1. D. Shockey, A. H. Marchand, S. R. Skaggs, G. E. Cort, M. W. Birckett and R. Parker, *Int. J. Impact Engng* **9**, 263 (1990).
2. D. J. Viechnicki, M. L. Slavin and M. I. Kliman, *Cer. Bull.* **70**, 1035 (1991).
3. J. Mescall, U. S. Materials Technology Laboratory, private communication (1988).
4. M. A. Meyers, *Dynamic Behavior of Materials*, p. 597, John Wiley, New York (1994).
5. J. W. Rudnicki and J. R. Rice, *J. Mech. Phys. Solids* **23**, 371 (1975).
6. I. Vardoulakis, *Int. J. Num. Analyt. Meth. Geomech.* **4**, 103 (1980).
7. I. Vardoulakis, *Int. J. Solids Struct.* **17**, 1085 (1981).
8. I. G. Vardoulakis and B. Graf, *IUTAM Conf. on Deformation and Failure of Granular Metals*, Delft, p. 485 (1982).
9. G. Scarpelli and D. M. Wood, *IUTAM Conf. on Deformation and Failure of Granular Metals*, Delft, p. 473 (1982).
10. I. Vardoulakis, *Acta Mechanica* **49**, 57 (1983).
11. J. Desrues, J. Lanier and P. Stutz, *Engng Fract. Mech.* **21**, 909 (1985).
12. H.-B. Mühlhaus and I. Vardoulakis, *Geotechnique* **37**, 271 (1987).
13. D. Kolymbas and G. Rombach, *Ingenieur-Archiv* **59**, 177 (1989).
14. J. P. Bardet, *J. Engng Mech.* **117**, 1466 (1991).
15. D. G. Schaeffer, *Proc. R. Soc. Lond. A* **436**, 217 (1992).
16. A. S. Saada, G. F. Bianchini and L. Liang, *Geotechnique* **44**, 35 (1994).
17. V. F. Nesterenko and M. P. Bondar, *DYMAT Journal* **1**, 245 (1994).
18. V. F. Nesterenko, M. A. Meyers, H. C. Chen and J. C. LaSalvia, *Appl. Phys. Lett.* **65**, 3069 (1994).
19. V. F. Nesterenko, M. A. Meyers, H. C. Chen and J. C. LaSalvia, *Metall. Mater. Trans. A* **26A**, 2511 (1995).
20. R. Prummer, *Proc. Emergent Process Methods for High Technology Ceramics: XIXth Univ. Conf.—Raleigh*, p. 1 (1983).
21. D. E. Grady and M. E. Kipp, *J. Mech. Phys. Solids* **35**, 95 (1987).
22. H. Ockendon and T. W. Wright, *Int. J. Plasticity* submitted.
23. V. F. Nesterenko, M. A. Meyers and T. W. Wright, *Acta metall. mater.* submitted (1995).
24. G. Scarpelli and D. M. Wood, *Proc. IUTAM Conf. on Deformation and Failure of Granular Materials*, Delft, p. 473. Balkema (1982).
25. A. N. B. Poliakov and H. J. Herrmann, *Geophys. Res. Lett.* **21**, 2143 (1994).

*Note added in proof:* Recent experiments by R. J. Clifton (private communication, 1995) on granular alumina suggest that the maximum shear strength is  $\sim 500\ \text{MPa}$ , at a superimposed stress of  $2\ \text{GPa}$ ; these results were obtained using the inclined plate impact technique. This value provides an estimate of maximum stress in Fig. 10; this, combined with the shear strains evaluated in the paper, enables a more quantitative description of the mechanical response of material investigated, taking into account the difference in the compressive stresses in the thick walled cylinder experiments [19] and in the inclined plate impact technique.